Analytical Methods

PAPER

View Article Online
View Journal | View Issue

Cite this: *Anal. Methods*, 2019, **11**, 1802

Chemical analysis using 3D printed glass microfluidics†

Eran Gal-Or,*[a] Yaniv Gershoni,[a] Gianmario Scotti,[b] Sofia M. E. Nilsson,[b] Jukka Saarinen,[b] Ville Jokinen,[bc] Clare J. Strachan,[b] Gustav Boije af Gennäs,[b] Jari Yli-Kauhaluoma[b] and Tapio Kotiaho*[bd]

Additive manufacturing (3D printing) is a disruptive technology that is changing production systems globally. In addition, microfluidic devices are increasingly being used for chemical analysis and continuous production of chemicals. Printing of materials such as polymers and metals is already a reality, but additive manufacturing of glass for microfluidic systems has received minor attention. We characterize microfluidic devices (channel cross-section dimensions down to a scale of 100 μm) that have been produced by additive manufacturing of molten soda-lime glass in tens of minutes and report their mass spectrometric and Raman spectroscopic analysis examples. The functionality of a microfluidic glass microreactor is shown with online mass spectrometric analysis of linezolid synthesis. Additionally, the performance of a direct infusion device is demonstrated by mass spectrometric analysis of drugs. Finally, the excellent optical quality of the glass structures is demonstrated with in-line Raman spectroscopic measurements. Our results promise a bright future for additively manufactured glass microdevices in diverse fields of science.

Received 3rd September 2018
Accepted 19th February 2019

DOI: 10.1039/c8ay01934g

rsc.li/methods

Introduction

Additive manufacturing (3D printing) technologies and their applications are advancing with unprecedented speed. For example, in medicine 3D bioprinting has allowed printing of tissues such as skin, bone and cartilage.[1–3] Custom made implants can also be made by additive manufacturing using X-ray or magnetic resonance imaging combined with 3D model design.[4,5] In the pharmaceutical field, additive manufacturing allows personalized medicine through drug dosage forms with personally tailored drug combinations, doses and drug release profiles.[6–8] In the chemical sciences, additive manufacturing is important for manufacturing miniaturized and microfluidic devices as chemical reactors or [bio]analytical devices.[8–14] Additive manufacturing of microelectronics is also possible.[15] Furthermore, additive manufacturing has allowed manufacturing of shape changing objects, with the shape transformation obtained, for example, by illumination with light.[16] In these cases, the term 4D printing has been used. Based on these examples, the main advantages of additive manufacturing stem from the fact that, after converting imaging data or visual observations and measurement data into a 3D computer design, the design can be easily and quickly transferred, with a single apparatus, to a desired complete product in a single step – assembly of multiple parts is typically not needed. Therefore, additive manufacturing enables rapid and affordable prototyping of devices and thus fast cycles of tool development and experiments.

The range of materials which can be used in additive manufacturing (3D printing) is extensive, including biomaterials (*e.g.* cells, protein, hydrogels), polymers (*e.g.* thermoplastics and photocurable polymers), ceramics and metals,[9] as well as multiple materials.[14,16] However, the lack of standardized biocompatible and transparent materials has been one of the main factors limiting the adoption of additive manufacturing for microfluidics.[10] Glass is one of the best materials for many chemical and biological applications, due to its excellent chemical and heat resistance, transparency, hardness, and high dielectric strength.[17] An additional advantage of glass,

[a]*MICRON3DP Ltd., IMC Group – ISCAR, Atir Yeda 21, Kfar-Saba 4464316, Israel. E-mail: eran.galor@micron3dp.com*

[b]*Drug Research Program, Division of Pharmaceutical Chemistry and Technology, Faculty of Pharmacy, P. O. Box 56 (Viikinkaari 5 E), FI-00014, University of Helsinki, Finland. E-mail: tapio.kotiaho@helsinki.fi*

[c]*Department of Chemistry and Materials Science, School of Chemical Engineering, P. O. Box 13500 (Aalto University), FI-00076 Aalto, Finland*

[d]*Department of Chemistry, Faculty of Science, P. O. Box 55, FI-00014, University of Helsinki, Finland*

† Electronic supplementary information (ESI) available: Cleaning of the microreactor; cleaning of the direct infusion device channel; Fig. S1–S9; linezolid synthesis and associated mass spectra with different reagent flow rates; offline mass spectrometry experiments: reagents for the offline MS, reaction conditions in the offline MS, offline MS measurement conditions; MS^n mass spectra and fragmentation schemes; electrospray ionization (ESI) mass spectra measured with the direct infusion device; validation of the purity of (5*S*)-5-(aminomethyl)-3-[3-fluoro-4-(4-morpholinyl)phenyl]-1,3-oxazolidin-2-one and linezolid (commercial reference compound): LC-MS analysis for the validation, ^{1}H NMR analysis for validation; movies; reference. See DOI: 10.1039/c8ay01934g

especially for chemical and biological measurement applications, is that the surface properties of glass can be easily tuned by well-known surface modification reactions.[18]

Such excellent properties have stimulated the development of additive manufacturing methods for glass. However, few examples consider the millimeter scale or below, *i.e.* going down to microfluidic dimensions and devices. One reason for this is the very high working temperature of glass (typically > 1000 K).[17] Glass may also crack due to intrinsic stresses induced during glass fabrication when not properly annealed. The major drawbacks for manufacturing of microfluidic glass devices by traditional microfabrication methods include the use of hazardous reagents, high instrumentation costs and challenges in bonding of glass layers.[19]

Two recent studies report additive manufacturing (3D printing) methods for transparent glass microfluidics based on the use of composite materials containing silica nanopowder: stereolithography[20,21] and direct ink writing.[22] Despite this progress in additive manufacturing of microfluidics, a very long heat treatment time (tens of hours) was needed in both studies for removal of solvent and organic binders of the composite material, as well as for sintering to obtain the final glass structure. Furthermore, since the method requires the outgassing of volatile binders, there is a limit to the wall thickness of the glass structures created with such methods, hampering their applicability. Recently, glass 3D printing using sol–gel technology[23] and a new fused silica glass subtractive machining technique based on a nanocomposite material have been introduced (microchannel structure shown).[24] However, both these methods also include a long heat treatment stage.

Selective laser-induced etching can be used to make 3D microfluidic glass structures, but it is not an additive manufacturing method since a laser is initially used to "draw" the structures in a glass specimen followed by wet-chemical etching to remove the exposed glass material.[25–28] This method is especially suited for quartz glass, and its precision is high (~10 μm).[26] However, production is generally limited to relatively short channels (~20 mm),[26,27,29] but it is possible to increase the channel length by using additional vertical entrances for the etching reagent.[30] Manufacturing of small devices is also possible with femtosecond laser ablation, often with the glass partly in water. However the resulting resolution and etching quality are worse than with subsequent chemical etching,[31] and microchannel lengths are typically limited to the cm range.[32,33] Femtosecond laser direct writing of porous glass and subsequent annealing allows manufacturing of microchannels with lengths of many centimeters and nanochannels with widths of tens of nanometers.[34–37]

In this study, we report characterization results and chemical applications of microfluidic devices (with a possible channel width down to ~100 μm) produced by additive manufacturing of molten glass (Fig. 1 and 2). This is the first full scientific study to report the devices and their characterization, it is a continuation of our preliminary report showing glass microreactors.[38] The additive manufacturing method used is a further development of the proprietary molten glass 3D printing technology developed at MICRON3DP.[39,40] Additive

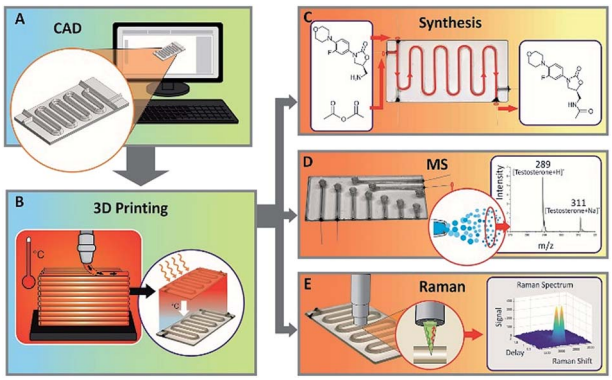

Fig. 1 Schematic of additively manufacturing (3D printing) microfluidics from molten glass and utilization of the microdevices in chemistry. (a) Designs of the microdevices are made using software for computer-aided design (*e.g.* Fusion 360), and (b) the microdevices are manufactured using an additive manufacturing device developed at MICRON3DP. Figures (c) to (e) show applications of the microdevices in online mass spectrometric analysis of a synthesis reaction, direct infusion mass spectrometric analysis of drugs and utilization of Raman spectroscopy as the in-line detection method for glass microfluidics, respectively.

manufacturing of molten transparent glass has also been reported by Oxman *et al.*, targeted mostly for architectural, artistic and industrial use.[41–43] In our study, functional operation of the additively manufactured microfluidic glass microreactor is demonstrated with online electrospray ionization (ESI) – mass spectrometric analysis of the last reaction step in the synthesis of linezolid, an antibiotic of last resort. In addition, operation of the additively manufactured glass direct infusion device is demonstrated by the analysis of selected drugs using electrospray-mass spectrometry. Moreover, the excellent optical quality of the additively manufactured glass structures is demonstrated by Raman spectroscopic measurements through the reactor channel wall.

Experimental

Reagents

(5*S*)-5-(Aminomethyl)-3-[3-fluoro-4-(4-morpholinyl)phenyl]-1,3-oxazolidin-2-one (also called linezolid related compound C, **1** in Fig. 3a and Scheme S1,† ≥97% purity) was obtained from Carbosynth Ltd. (Compton, UK). Acetic anhydride (≥99% pure, compound **2**, in Fig. 3a and Scheme S1†), linezolid (≥98% pure, compound **3**, in Fig. 3a and Scheme S1†), verapamil hydrochloride (98%), testosterone (≥99%), cyclohexane (≥99.8% pure) and ethyl acetate (≥99.5% pure) were purchased from Sigma-Aldrich (Steinheim, Germany). Formic acid (98–100%) was obtained from Merck Chemicals GmbH (Darmstadt, Germany). The purity of (5*S*)-5-(aminomethyl)-3-[3-fluoro-4-(4-morpholinyl)phenyl]-1,3-oxazolidin-2-one and linezolid were verified using LC-MS and ^{1}H NMR (only the starting material), as described in the ESI† (page 24). Chromasolv®-grade acetonitrile and Chromasolv®-grade methanol were purchased from Honeywell (Morris Plains, USA). Hydrogen peroxide (30% w/w in water, stabilized with dipicolinic acid) was obtained from

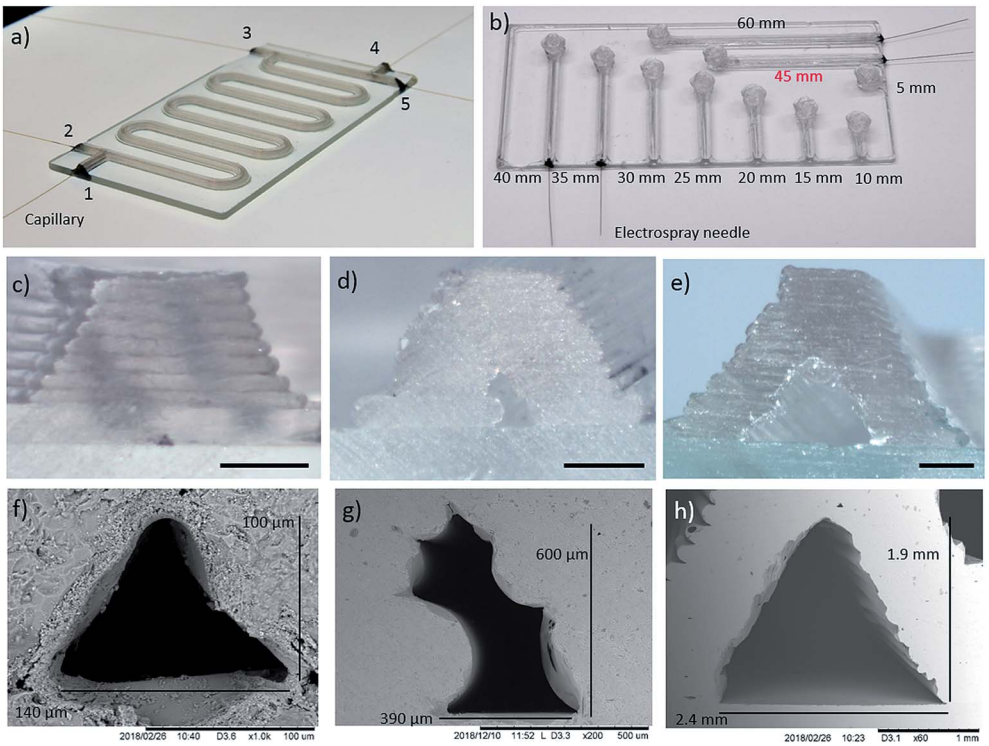

Fig. 2 Glass microfluidic devices. (a) Microreactor device (glass base plate size 100 × 50 × 2 mm^3, total channel length ~400 mm), mid-size cross-section. All inlets include glued silica capillaries. (b) Direct infusion device (glass base plate size 100 × 50 × 1 mm^3, 45 mm channel used in the MS measurements). Four channels have a glued stainless steel electrospray needle. Optical micrographs of the cross-sections of (c) a small channel (microreactor in S3), (d) a mid-size channel (microreactor in a) and (e) a large channel (reactor in S3). The black dipstick (1 mm) in the optical channel end micrographs is shown only to demonstrate the size range of the channels (for more precise dimensions, see the SEM-pictures). Scanning electron micrographs of (f) a small channel (microreactor in S3), (g) a mid-size channel (microreactor in a) and (h) a large channel (an example large channel piece). Brightness and contrast of the images a and b have been edited to increase visibility of the additively manufactured glass devices.

Riedel-de Haën, distributed by Honeywell (Morris Plains USA). The water used for direct infusion experiments, cleaning of the reactor, and preparing the diluted hydrogen peroxide solution was purified with a Milli-Q Plus purification system from Millipore (Molsheim, France). Dimethyl sulfoxide-d_6 (DMSO-d_6, 100%, 99.96 atom% D) obtained from Sigma-Aldrich (Steinheim, Germany) was used in the NMR experiments.

Additive manufacturing (3D printing) of the glass devices

Additive manufacturing of molten glass is a proprietary technology of MICRON3DP.[44–46] The technology is especially designed for 3D printing of materials with a high melting temperature. The technology includes parts such as a heated chamber inside which printing is performed such that thermal stress does not cause cracks, a printing nozzle (lower part inside the heated chamber) and its heating system, a printing base plate mounted inside the heated chamber, a cooling unit for cooling the upper part of the printing nozzle (outside the heated chamber), a system for precise movement of the printing nozzle and/or the printing base plate and a loading system for printing material allowing, for example, printing of different glass colors and continuous printing to avoid cracks. Further details about the manufacturing of the glass devices is discussed in the first paragraph of the Results and discussion section.

Mass spectrometric (MS) set-up and conditions for the reaction studies

The MS measurement set-up is shown in Fig. S1.† Deactivated fused silica capillaries (OD 190 µm (based on caliper (0–25 × 0.01 mm) measurement 180 to < 190 µm), ID 75 µm, length between 320 mm and 370 mm, Trajan Scientific Europe, Milton Keynes, UK) were attached to the additively manufactured glass reactor by inserting them into the inlets and gluing them (capillaries after gluing ~3–11 mm inside the channels) with Duralco 4703 (Cotronics Corp., Brooklyn, USA), a highly thermally and chemically stable epoxy glue. The edge of the microreactor (Fig. 2a) required grinding in some places to reach the channels for silica capillary insertion. The microreactor has in total five inlet/outlets, two at one end of the base plate, and three at the other end of the base plate (Fig. 2a). In the online experimental results presented (Fig. 3 and S10†), the inlet/outlet 1 was plugged with epoxy, and the inlet/outlet 2 was used as the reaction solution outlet (reaction channel length ~360 to 380 mm). The reaction solution was conducted *via* the fused silica capillary to the ion source of an ion trap mass spectrometer. The fused silica capillaries of inlets/outlets 4 and 5 were used (compound **2** from 4 and compound **1** from 5) for reagent infusion into the microreactor. The capillary connected to inlet/outlet 3 was in this experiment blocked with a column plug and

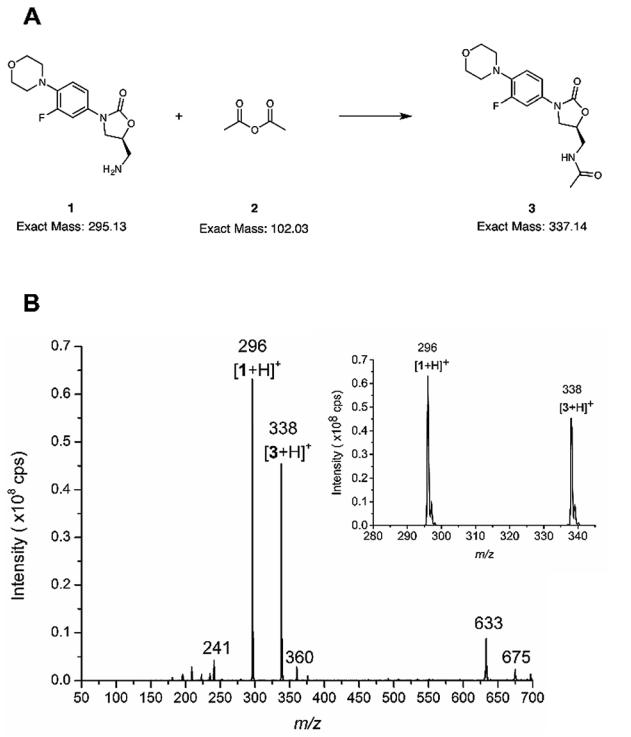

Fig. 3 Reaction analysis by online mass spectrometry. (a) The reaction between (5*S*)-5-(aminomethyl)-3-[3-fluoro-4-(4-morpholinyl) phenyl]-1,3-oxazolidin-2-one (**1**) and acetic anhydride (**2**) to produce linezolid (**3**), (b) mass spectra averaged over 1 min at the reactant infusion flow rate 750 nL min^{-1} per reactant (total flow 1.5 μL min^{-1}). The inset shows the same spectrum as the full *m*/*z* scan range spectrum, but only in a *m*/*z* range where the analytes of interest ($[1 + H]^+$, at *m*/*z* 296 and $[3 + H]^+$, at *m*/*z* 338) are present.

a union (IDEX Europe GmbH, Erlangen, Germany). An alternative measurement arrangement was also used, in which inlets/outlets 1 and 2 were used for reagent infusion, inlets/outlets 4 and 5 were plugged with column plugs and unions (IDEX Europe GmbH, Erlangen, Germany) and the capillary of inlet/outlet 3 was used to conduct the reaction solution to the ion trap mass spectrometer (reaction channel length ~330–350 mm). The two reagent introduction silica capillaries were connected to separate 1 mL syringes (ID 4.6 mm, Hamilton Bonaduz AG, Bonaduz, Switzerland) by fittings and unions (IDEX Europe GmbH, Erlangen, Germany). A PHD 2000 syringe pump (Harvard Apparatus, Holliston, USA) was used for infusing the solvents and/or reagents into the reactor.

MS measurement conditions in the reaction studies

The outlet of the glass microreactor was coupled to a commercial electrospray ionization source of an Agilent 6330 ion trap (Agilent Technologies, Santa Clara, USA). The ion trap was operated in positive mode, with the capillary voltage −3 kV. Nitrogen was used as drying gas and introduced with a flow rate of 4 L min^{-1}. The drying gas temperature was 300 °C and the *m*/*z* scan range was 50–600 or 50–700 for the MS and MS^n experiments. Mass spectra were recorded continuously during the online experiments, and the presented mass spectra are the average over 1 min at time points when the ion currents for the used flow rate had stabilized. The integer value of the precursor ion was isolated for the MS^n experiments with the isolation width 1.0 *m*/*z*. MS^n data was recorded for 30 s for each precursor ion and the product ion mass spectra were averaged over this time. The mass spectrometric data was processed with the software DataAnalysis for 6300 series ion trap LC/MS version 3.4, Build 192 (Agilent Technologies, Santa Clara, USA).

Reaction conditions

Initially, the additively manufactured microreactor was filled with Chromasolv®-grade acetonitrile by infusing it through two of the inlets with 1 mL syringes using typically the first or the only infusion flow rate in the online reaction experiment to record a background mass spectrum (a mass spectrum of the solvent used for preparing the samples without reagents). After this, the online reaction studies were conducted. A 1 mL syringe was filled with a 100 μM solution of (5*S*)-5-(aminomethyl)-3-[3-fluoro-4-(4-morpholinyl)phenyl]-1,3-oxazolidin-2-one in acetonitrile and another one with a 100 μM solution of acetic anhydride in acetonitrile. This procedure gives the concentration of 50 μM per reagent at the beginning of the glass reactor channel. Solutions producing reagent concentrations of 170 and 10 μM at the beginning of the glass reactor were also tested (MS spectra not reported). The syringes were coupled to the separate inlets of the glass reactor as described above in the MS measurement set-up section and the mass spectrometric data acquisition started. Infusion flow rates of 4.0 μL min^{-1}, 1.6 μL min^{-1} and 750 nL min^{-1} per syringe were used, giving total flow rates through the reactor of 8.0, 3.2 and 1.5 μL min^{-1}, respectively. Reaction experiments using only one total flow rate and experiments in which the total flow rate was decreased (8.0, 3.2 and 1.5 μL min^{-1}) during the same measurement time were performed. All reaction experiments were conducted at room temperature. Mass spectra were recorded continuously during the reaction experiments and averaged at time points when the signal represented the stabilized infusion flow rate. Of note, in the experiments in which the flow rates decreased during the experiment, there are delay times before the observed signals stabilized to the characteristic level of each flow rate.

In addition to the online experiments, pure (5*S*)-5-(aminomethyl)-3-[3-fluoro-4-(4-morpholinyl)phenyl]-1,3-oxazolidin-2-one (**1**) and pure linezolid (**3**) (typically each 50 μM in acetonitrile) were analyzed by direct infusion electrospray ionization mass spectrometry using the same MS operating settings as for the online reaction study. This was done to collect reference MS and MS^n data for these compounds.

Mass spectrometric set-up and conditions for the direct infusion experiments

Stainless steel nano-ESI needles (length 30 mm, OD 150 μm, ID 30 μm Thermo-Fisher Scientific Oy, Vantaa, Finland) were glued in the channels of the direct infusion device with Duralco 4703 (Cotronics Corp., Brooklyn, USA) (Fig. 2b). The direct infusion device was positioned in front of the capillary extension of an Agilent 6330 ion trap using an *xyz*-stage (Märzhauser Wetzlar

GmbH & Co. KG, Wetzlar, Germany) attached to an ion source frame. One end of a copper wire was wrapped around the nano-ESI needle, while its other end was wrapped around a metal rod of the ion source frame to ground the nano-ESI needle.

MS settings for the direct infusion experiments

The Agilent 6330 ion trap (Agilent Technologies, Santa Clara, USA) was operated in positive ESI mode, using a capillary voltage of −3 kV. The temperature of the drying gas (nitrogen) was 100 °C, and the flow rate of the drying gas was 2 L min^{-1}. The used m/z scan range was 50–600. The presented mass spectra are the average over 1 min.

Measurement conditions for the direct infusion experiments

Solutions of 10 μg mL^{-1} verapamil hydrochloride (20 μM) and testosterone (35 μM) in a mixture of Chromasolv®-grade methanol : water 80 : 20 + 1 vol% formic acid were prepared, respectively. The channel (45 mm channel in Fig. 1d and 2b) of the direct infusion device was filled with the sample mixture by manual direct infusion using a 1 mL syringe (ID 4.6 mm, Hamilton Bonaduz AG, Bonaduz, Switzerland). Complete filling of the channel was confirmed by filling the channel until it was flooded, visually ensuring that there were no air bubbles in the channel (and in case of air bubbles, the device was tilted vertically so that the air bubbles could exit at the infusion inlet, after which the device was again filled with direct manual infusion), and finally depositing a droplet of the sample mixture at the sample reservoir. When the filled device was positioned in front of the mass spectrometer inlet, acquisition of mass spectra was initiated, the capillary voltage of the mass spectrometer was switched on and optimization of the positioning of the device in front of the mass spectrometer was done until a stable electrospray current was obtained. In all the experiments of sufficient quality with this device, the capillary current of the mass spectrometer was below 100 nA.

Raman spectroscopy

A time-gated Raman spectrometer was used to measure the Raman spectra (TimeGated® 532, TimeGate Instruments, Oulu, Finland). The system consisted of a 532 nm picosecond pulsed laser (pulse width < 100 ps, repetition rate 40–50 kHz, average output power approximately 60 mW), sampling optics (fiber), spectrometer with a complementary metal-oxide-semiconductor (CMOS) single-photon avalanche diode (SPAD) detector (8 cm^{-1} spectral resolution) and a computer with MATLAB-based measurement software (MathWorks, Massachusetts, USA). A sampling probe (BWTek Raman Probe, B&W Tek, Newark, USA) with a focal distance of 5 mm and spot size of approximately 85 μm was used.

Reference spectra of cyclohexane and ethyl acetate were measured in a 4 mL glass vial (through the glass). For the microreactor device (Fig. 2a) measurements, the sampling probe was placed above the channel in the glass microreactor (Fig. S2†). Spectra without solvent and then with cyclohexane or ethyl acetate were measured from 700 to 1500 cm^{-1} and 2600 to 3200 cm^{-1} from the same spot. The solvents were infused into the glass reactor using syringe pumps (Harvard Apparatus, Pump 11 Elite and PHD 2000, Massachusetts, USA, in Fig. S2† only one pump shown) and 1 mL syringes with an infusion rate of 5 μL min^{-1}. The time-resolved spectral datasets, including Raman and photoluminescence signals, were collected with the time gate sequentially moved in 50 ps steps using the electronic delay generator from 0 to 2 ns. The processed sum Raman spectra consisted of six such cycles and the time window of 0.2 to 0.7 ns was used when fluorescence subtraction was performed. Min–max normalization was also applied. The total measurement time for each sample was approximately 6 min. The measurements were carried out at ambient temperature, lighting and humidity.

Microscopy

To obtain the channel cross-section images, either intact glass devices, or glass channel cross-section samples, were used. For optical microscopy, an object of known size, included in the image was used to obtain the scale bar. For scanning electron microscopy (TM-1000, Hitachi, Tokyo, Japan), the samples were coated with gold by sputtering (Bal-Tec SCD 050, Schalksmühle, Germany). The sputtering voltage was 60 mA and the time was 60 s.

Surface roughness measurements

Surface roughness of the additively manufactured glass microreactors was characterized with a Dectak XT (Bruker, Germany) stylus profilometer.

Results and discussion

Fig. 1 illustrates the concept of additively manufacturing (3D printing) microfluidics from molten glass. Using a custom STL to G-code technique, MICRON3DP can manufacture glass channels as narrow as 100 μm (Fig. 2). The software-based designs can be modified during manufacturing to reduce the cross-section and increase the yield of glass devices. When the final printing model does not contain holes at the end of the channels, the rims of the manufactured microfluidic parts are cut away to open the channels. The glass additive manufacturing process is carried out directly on a glass plate inside a heated chamber, thus preventing thermal shock (Fig. 1b). The manufacturing temperature for the soda-lime glass was 1000 °C in the present study. Manufacturing (printing) times are typically on a time-scale of minutes. For example, the object presented in the movie[38] was additively manufactured in 15 min. In addition to the time needed for additive manufacturing, there is an annealing time of approximately 20 to 30 min, which is calculated based on the glass volume manufactured. Soon after the annealing, the product can be used. Multiple microfluidic tools can be printed on the same glass base plate in one print job. A movie showing additive manufacturing of glass is presented in the ref. 40.

Two prototype devices were designed to demonstrate both the printing capabilities and the performance in synthetic and analytical chemistry microfluidic applications. An additively

manufactured microreactor device is presented in Fig. 2a (glass base plate size 100 × 50 × 2 mm^3). The microreactor device has two reagent inlets/outlets at one end and three inlets/outlets at the other end. The three-inlet/outlet topology can be used for addition of a dilution solvent, another reagent or a quenching reagent. The total length of the channel is approximately 400 mm. This geometry is useful, for example, for the analysis of reactions that need higher reagent concentrations than the online analytical equipment can tolerate. Microreactor devices with the same design, but with smaller and larger channel cross-sections are shown in Fig. S3.† However, the fluidic functionality and leak tightness of these devices was not tested. The second design was a direct infusion device (Fig. 2b and S8,† glass base plate size 100 × 50 × 1 mm^3), which has a straight channel with a sample reservoir at the other end. The channels with a glued electrospray needle have lengths ranging from 35 to 60 mm, from which the 45 mm channel was used for mass spectrometric experiments. The direct infusion devices show that small glass channels can be additively manufactured for direct infusion electrospray ionization mass spectrometry. In addition, a third design manufactured was a spiral device (Fig. S9†), this contains an extremely long single channel (~2.5 m) with an inlet/outlet at each end. The integrity of the spiral device was tested by pumping air through it when the device was submerged under water. The ESI movies (Movies S1 and S2†) reveal air bubbles emerging from the exit as well as from the inlet side. Altogether, these devices demonstrate the versatility of additive manufacturing with molten glass. Neither the channel length nor the sidewall thickness is limited, unlike with techniques requiring either development or outgassing steps. Furthermore, 3D shapes including 90° vertical turns can be manufactured as demonstrated by the devices in Fig. 2b and S9.†

The geometries and sizes of microchannel cross-sections were examined with optical and electron microscopy. Fig. 2c–h shows example cross-sections for the manufactured glass devices. The smallest channel (Fig. 2c and f) has a triangle cross-section with a width of ~140 μm and a height of ~100 μm. The mid-size channel (Fig. 2d and g), has a "tilted rectangle" cross-section with a width and height of roughly 400 and 600 μm, respectively. The largest channel (Fig. 2e and h) has a triangular cross-section and is about 2 mm wide and high. The cross-section shape and size variation is demonstrated for the small channel reactor (Fig. S3) in Fig. S4,† the mid-size channel microreactor (Fig. 2a) in Fig. S5 and S6,† and the large channel structure (Fig. S3) in Fig. S7.† In addition, the size and shape variation of the channel ends of the direct infusion device (Fig. 2b) are presented in Fig. S8.† As can be seen from Fig. S4–S7,† the channel size and shape within a glass device are similar in the entire device and it is possible to manufacture different channel shapes (see Fig. S4–S8† for comparison).

The surface roughness of the outer surface of the microreactors was characterized by placing the tip of a stylus profilometer on the top of a channel and scanning longitudinally. The surface was scanned over 400 μm at 10 different spots to obtain the average roughness, R_a, and root mean square (RMS) roughness, R_q. This resulted in R_a and R_q averages of 47 nm and 58 nm respectively, with their corresponding standard deviations being 17 nm and 22 nm, respectively. We assume that these numbers represent the surface roughness of one glass layer, which should be on the same order of magnitude on the outside and inside of the channels, since molten glass is printed. Undulation in the channel wall structure (see Fig. 2c–e, and S4–S8†) is believed to be caused by the glass layer thickness.

The total volume of the mid-size microreactor device (Fig. 2a) was calculated from the overall channel length of ~400 mm and the cross-sectional dimensions (the cross-section area estimated as the average of four channel (Fig. S6†) cross-sections is 0.124 mm^2 with STD of 0.015 mm^2) obtained from the electron micrographs. The volume calculated in this way was 50 μL. A larger volume, approximately 65–70 μL, was obtained for the total measurement system (reaction channel length ~360–380 mm and connections to syringe pump and to MS; see microreactor in Fig. 2a and set-up in S1†) used for online mass spectrometric reaction experiments. This estimation is based on the reaction solution flow rate and the delay after introducing the reagents until detection of reagent (**1**) and final product (**3**) by mass spectrometry.

All in all, there are five key advantages of the glass additive manufacturing method developed and used: (1) fabrication of microchannel dimension as low as 100 μm (Fig. 2f), (2) the ability to print large complete devices (sizes up to 200 × 200 × 350 mm^3) on top of a glass base plate, (3) the ability to print very long microchannels (Fig. 2a (400 mm) and S9† (2.5 m)), (4) only the layer dimensions are limiting the sidewall thickness, and (5) rapid manufacture of microfluidic devices (within tens of minutes instead of tens of hours). Additive manufacturing of different glass qualities (soda-lime, borosilicate) and colored glass is also possible, even though in this study the microfluidic devices were limited to clear soda-lime glass. These unique additive manufacturing characteristics are based on recently developed printer nozzle and heating system structures.

The microreactor (Fig. 2a) was used for online analysis of the last step in the synthesis of linezolid (Fig. 3a)[47] by infusing (5*S*)-5-(aminomethyl)-3-[3-fluoro-4-(4-morpholinyl)phenyl]-1,3-oxazolidin-2-one, reagent **1**, through one of the microreactor inlets and acetic anhydride, **2**, (both dissolved in acetonitrile) through another inlet and conducting the reaction solution *via* an outlet directly to an ion trap for continuous mass spectrometric analysis. The mass spectrum presented in Fig. 3 is from an experiment in which the initial reagent flow rate of 4.0 μL min^{-1} per reagent (total flow 8.0 μL min^{-1}) was decreased in two steps, first to 1.6 μL min^{-1} per reagent (total flow 3.2 μL min^{-1}) and then down to 750 nL min^{-1} per reagent (total flow rate 1.5 μL min^{-1}). A mass spectrum with the reagent infusion flow rate of 750 nL min^{-1} is presented in Fig. 3b and mass spectra with reagent infusion flow rates of 4.0 μL min^{-1} and 750 nL min^{-1} are shown in Fig. S10.† Protonated molecules of both reagent **1** and the final product **3** can been seen in these mass spectra at *m*/*z* ratios of 296 and 338, respectively. Another observation was that the intensity of the protonated linezolid reaction product $[\mathbf{3} + H]^+$ increases in relation to the protonated reagent $[\mathbf{1} + H]^+$ at *m*/*z* 296, as the reaction time increases due the decreased reagent infusion flow rate (Fig. S10†). The offline

experiment (reaction in a vial) showed the same trend, *i.e.* the signal of protonated linezolid, $[\mathbf{3} + H]^+$ increases in relation to $[\mathbf{1} + H]^+$ as the reaction time increases (Fig. S12†). MS^n (multiple-stage mass spectrometry) mass spectra and the proposed fragmentation routes for the *m*/*z* 296 and 338 are presented in the ESI† (Fig. S13–S15, Schemes S2 and S3†). Other reaction related ions present and tentatively identified in the mass spectra (Fig. 3b and S10†) are: *m*/*z* 241, a fragment of *m*/*z* 296 formed in the ionization process; *m*/*z* 360, $[\mathbf{3} + Na]^+$; *m*/*z* 633, $[\mathbf{1} + \mathbf{3} + H]^+$; and *m*/*z* 675, $[\mathbf{3} + \mathbf{3} + H]^+$.

The direct infusion device (Fig. 2b) was used for measuring mass spectra of verapamil and testosterone using electrospray ionization mass spectrometry. The electrospray was achieved with a help of a stainless steel nanospray needle glued into the direct infusion device. The length of the channel used in this experiment was 45 mm. Protonated verapamil and testosterone at *m*/*z* 455 and 289, respectively, were clearly seen in the mass spectra (Fig. S16†).

The potential of optical detection for in-line analysis with additively manufactured glass devices was studied by measuring Raman spectra of cyclohexane and ethyl acetate through the channel of the microreactor device (Fig. 2a, 4 and S2†). The Raman spectrum of the empty glass reactor contained a broad peak centered at 1112 cm^{-1} which is associated with stretching of the Si–O– non-bridging and Si–O–Si bridging groups (Fig. 4a).[48,49] No bands were present between 2600–3200 cm^{-1} (Fig. 4a). With the exception of the mode centered around 1112 cm^{-1}, the additively manufactured glass otherwise exhibits minimal Raman scattering and consequent interference in the spectral regions of interest for organic system analyses.[50]

Cyclohexane exhibited a strong symmetric CH_2 stretching mode at 2855 cm^{-1} and two antisymmetric CH_2 stretching modes at 2928 cm^{-1} and 2942 cm^{-1} (Fig. 4b (vial) and 4c (microreactor)).[51] Ethyl acetate exhibited a strong CH_3 stretching signal at 2948 cm^{-1} (Fig. 4b (vial) and 4c (microreactor)). The small solvent sampling volume affected the observed Raman signal intensities of the solvents. Nevertheless, the signals showed that such additively manufactured reactors have sufficient optical transparency for non-invasive in-line Raman measurements.

Time-gated Raman spectroscopy (Fig. 4d–i) has the further advantage that Raman spectra can be efficiently obtained in the presence of fluorescence and other photoluminescent phenomena.[52,53] This is achieved through temporal rejection of the fluorescence signal, which, unlike the near instantaneous Raman signal, typically occurs on the order of nanoseconds (or even longer).[54] This expands the range of possible glass materials (*e.g.* soda-lime glass) for printing, without concern for their photoluminescent properties. Efficient fluorescence rejection

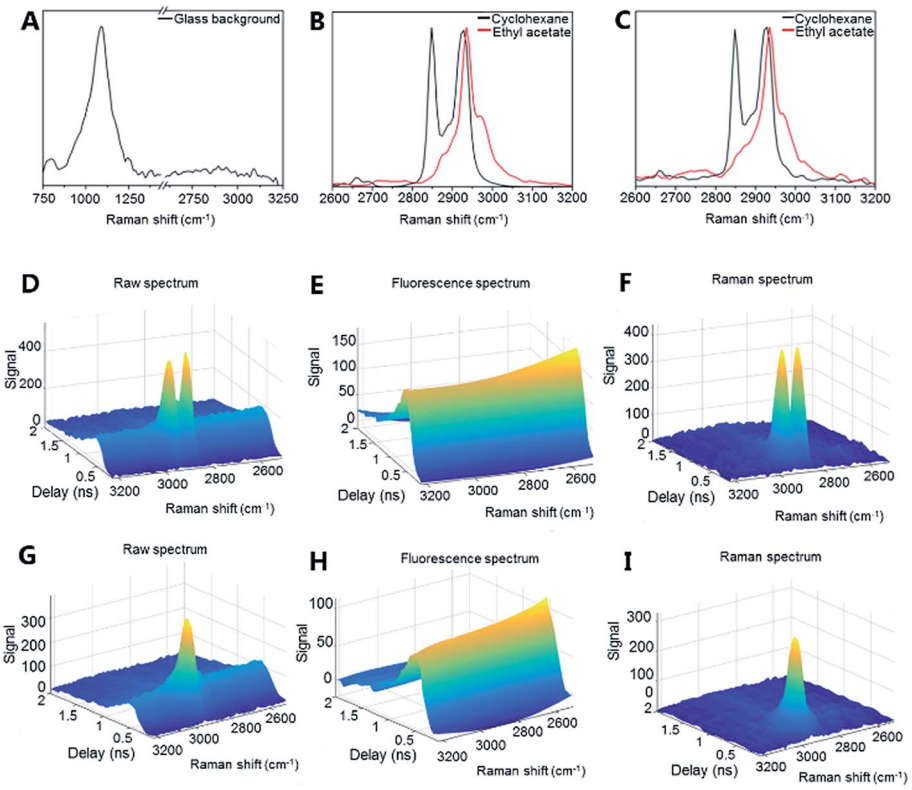

Fig. 4 Optical detection by Raman spectroscopy. (a) Raman spectrum of the empty glass microreactor, (b) cyclohexane and ethyl acetate in a glass vial, (c) cyclohexane and ethyl acetate in the glass microreactor. The data was obtained with time-gated Raman spectroscopy. Raman spectra can be obtained in the presence of fluorescence through time-gating and after subtracting the fluorescence (baseline) spectrum from the raw data as demonstrated for cyclohexane in figures (d) to (f) and ethyl acetate in (g) to (i). The detection time-window of 0.2 to 0.7 ns was used to generate the 2D Raman spectra from the raw data. Min–max normalization was applied for clarity in (a) to (c).

also makes the non-contact sampling optics more flexible – here a simple non-contact fiber-optic Raman probe with a theoretical spot size of approximately 85 μm has been used and sampling could be performed directly through the printed glass. To date, non-contact sampling in glass microfluidic systems has generally involved microscope objectives and optimized selection of the bottom glass plate material through which the non-contact sampling has been performed.[55] Furthermore, time-gated instrumentation allows measurements to be performed in ambient lighting without interference. The present results demonstrate that Raman (and other optical) analysis is possible with additively manufactured glass microfluidic set-ups. The sensitivity of the Raman analysis (*e.g.* for complex mixtures and low concentration components) could be further optimized by, for example, modifying the microfluidic device geometry and increasing the Raman scattering signal intensity with, for example, surface enhanced Raman scattering (SERS) approaches.[50]

Conclusions

True additive manufacturing, 3D printing, of microfluidic (channels < 500 μm) devices from molten glass has been demonstrated. The main advantages of the devices stem from the excellent properties of glass for chemical and biological applications and the fact that large complete devices can be manufactured in tens of minutes. The latter property is especially important when one considers the advantages of 3D printing such as custom manufacturing and rapid prototyping. The applicability of one of the devices was shown with online mass spectrometric analysis of the last reaction step in the synthesis of linezolid, while another was used for direct infusion MS measurements of drugs. The excellent optical quality of the additively manufactured glass was demonstrated by measuring the Raman spectra of solvents. Relevant optical technologies include fluorescence, Raman, and UV spectroscopies as well as colorimetry. The optical sampling possibilities are diverse: depending on the optical technique, measurements could be performed in the backwards (including through the base-plate) or transmission (forwards) directions anywhere along the microchannel path. There is also potential for simultaneous measurements at different positions along the channels as well as imaging. We see a bright future for these micrometer or millimeter scale glass devices, for example, in flow chemistry, an area of chemistry with large commercial success. In addition, applications in analytical and medicinal chemistry, biology and biochemistry are likely to result from this study.

Conflicts of interest

MICRON3DP has a commercial interest in the results.

Acknowledgements

Chief technician Matti Hongisto from Clinicum, Faculty of Medicine, University of Helsinki is acknowledged for help with glass drilling. Nina Sipari and Dr Jenna Lihavainen, University of Helsinki are acknowledged for the LC-MS measurements. Expert help from Sole Lätti in graphical illustration is acknowledged. The facilities of Micronova, Centre for Micro and Nanotechnology were used in the characterization. Financial support for the University of Helsinki was provided by the Academy of Finland (projects 276627, 265481 and 289398), Ruth and Nils-Erik Stenbäck's Foundation and Magnus Ehrnrooth's Foundation.

References

1 S. V. Murphy and A. Atala, *Nat. Biotechnol.*, 2014, **32**, 773–785.
2 C. Mandrycky, Z. Wang, K. Kim and D.-H. Kim, *Biotechnol. Adv.*, 2016, **34**, 422–434.
3 M. Nowicki, N. J. Castro, R. Rao, M. Plesniak and L. G. Zhang, *Nanotechnology*, 2017, **28**, 382001.
4 S. L. Sing, J. An, W. Y. Yeong and F. E. Wiria, *J. Orthop. Res.*, 2016, **34**, 369–385.
5 F. Rengier, A. Mehndiratta, H. von Tengg-Kobligk, C. M. Zechmann, R. Unterhinninghofen, H.-U. Kauczor and F. L. Giesel, *Int. J. Comput. Assist. Radiol. Surg.*, 2010, **5**, 335–341.
6 S. A. Khaled, J. C. Burley, M. R. Alexander, J. Yang and C. J. Roberts, *Int. J. Pharm.*, 2015, **494**, 643–650.
7 J. Goole and K. Amighi, *Int. J. Pharm.*, 2016, **499**, 376–394.
8 A. J. Capel, R. P. Rimington, M. P. Lewis and S. D. R. Christie, *Nat. Rev. Chem.*, 2018, **2**, 422–436.
9 B. Gross, S. Y. Lockwood and D. M. Spence, *Anal. Chem.*, 2017, **89**, 57–70.
10 N. Bhattacharjee, A. Urrios, S. Kang and A. Folch, *Lab Chip*, 2016, **16**, 1720–1742.
11 A. K. Au, W. Huynh, L. F. Horowitz and A. Folch, *Angew. Chem., Int. Ed.*, 2016, **55**, 3862–3881.
12 Y. He, Y. Wu, J.-z. Fu, Q. Gao and J.-j. Qiu, *Electroanalysis*, 2016, **28**, 1658–1678.
13 C. K. Dixit, K. Kadimisetty and J. Rusling, *TrAC, Trends Anal. Chem.*, 2018, **106**, 37–52.
14 F. Li, N. P. Macdonald, R. M. Guijt and M. C. Breadmore, *Lab Chip*, 2019, **19**, 35–49.
15 R. D. Sochol, E. Sweet, C. C. Glick, S.-Y. Wu, C. Yang, M. Restaino and L. Lin, *Microelectron. Eng.*, 2018, **189**, 52–68.
16 R. L. Truby and J. A. Lewis, *Nature*, 2016, **540**, 371–378.
17 B. H. W. S. De Jong, R. G. C. Beerkens, R. A. van Nijnatten and E. Le Bourhis, Glass, 1. Fundamentals, in *Ullmann's Encyclopedia of Industrial Chemistry*, Wiley-VCH Verlag GmbH & Co. KGaA, Weinheim, 2011, pp. 1–54.
18 M. D. Sonawane and S. B. Nimse, *Journal of Chemistry*, 2016, 9241378.
19 K. Ren, J. Zhou and H. Wu, *Acc. Chem. Res.*, 2013, **46**, 2396–2406.
20 F. Kotz, K. Plewa, W. Bauer, N. Schneider, N. Keller, T. Nargang, D. Helmer, K. Sachsenheimer, M. Schäfer, M. Worgull, C. Greiner, C. Richter and B. E. Rapp, *Adv. Mater.*, 2016, **28**, 4646–4650.
21 F. Kotz, K. Arnold, W. Bauer, D. Schild, N. Keller, K. Sachsenheimer, T. M. Nargang, C. Richter, D. Helmer and B. E. Rapp, *Nature*, 2017, **544**, 337–339.

22 D. T. Nguyen, C. Meyers, T. D. Yee, N. A. Dudukovic, J. F. Destino, C. Zhu, E. B. Duoss, T. F. Baumann, T. Suratwala, J. E. Smay and R. Dylla-Spears, *Adv. Mater.*, 2017, **29**, 1701181.

23 J. F. Destino, N. A. Dudukovic, M. A. Johnson, D. T. Nguyen, T. D. Yee, G. C. Egan, A. M. Sawvel, W. A. Steele, T. F. Baumann, E. B. Duoss, T. Suratwala and R. Dylla-Spears, *Adv. Mater. Technol.*, 2018, **3**, 1700323.

24 F. Kotz, N. Schneider, A. Striegel, A. Wolfschläger, N. Keller, M. Worgull, W. Bauer, D. Schild, M. Milich, C. Greiner, D. Helmer and B. E. Rapp, *Adv. Mater.*, 2018, **30**, 1707100.

25 F. He, Y. Liao, J. Lin, J. Song, L. Qiao, Y. Cheng and K. Sugioka, *Sensors*, 2014, **14**, 19402–19440.

26 J. Gottmann, M. Hermans, N. Repiev and J. Ortmann, *Micromachines*, 2017, **8**, 110.

27 P. Paiè, F. Bragheri, D. Di Carlo and R. Osellame, *Microsyst. Nanoeng.*, 2017, **3**, 17027.

28 F. Sima, K. Sugioka, R. Martínez Vázquez, R. Osellame, L. Kelemen and P. Ormos, *Nanophotonics*, 2018, **7**, 613–634.

29 C. Weingarten, S. Steenhusen, M. Hermans, E. Willenborg and J. H. Schleifenbaum, *Microfluid. Nanofluid.*, 2017, **21**, 165.

30 S. Ho, P. R. Herman and J. S. Aitchison, *Appl. Phys. A*, 2012, **106**, 5–13.

31 Y. Bellouard, Laser-based micro- and nanoprocessing IX, in *Proceedings of SPIE*, ed. U. Klotzbach, K. Washio and C. B. Arnold, 2015, vol. 9351, p. 93510G.

32 K. Sugioka, J. Xu, D. Wu, Y. Hanada, Z. Wang, Y. Cheng and K. Midorikawa, *Lab Chip*, 2014, **14**, 3447–3458.

33 D. J. Hwang, T. Y. Choi and C. P. Grigoropoulos, *Appl. Phys. A: Mater. Sci. Process.*, 2004, **79**, 605–612.

34 Y. Cheng, *Micromachines*, 2017, **8**, 59.

35 C. Liu, Y. Liao, F. He, J. Song, D. Lin, Y. Cheng, K. Sugioka and K. Midorikawa, *J. Laser Micro/Nanoeng.*, 2013, **8**, 170–174.

36 Y. Liao, Y. Ju, L. Zhang, F. He, Q. Zhang, Y. Shen, D. Chen, Y. Cheng, Z. Xu, K. Sugioka and K. Midorikawa, *Opt. Lett.*, 2010, **35**, 3225–3227.

37 Y. Liao, Y. Cheng, C. Liu, J. Song, F. He, Y. Shen, D. Chen, Z. Xu, Z. Fan, X. Wei, K. Sugioka and K. Midorikawa, *Lab Chip*, 2013, **13**, 1626–1631.

38 E. Gal-Or, Glass 3D printing of microfluidics tools, https://www.linkedin.com/pulse/glass-3d-printing-microfluidics-tools-eran-gal-or/, 18.07.2017, accessed August 2018 and movie Custom microfluidic tool by MICRON3DP glass 3d printing, https://www.youtube.com/watch?v=DEJgEjqqU90, accessed August 2018. Additive manufacturing (3D printing) of the experimental microfluidic (in the movie) part with 500 μm channels width: After modeling the final part, the 3D model was 'sliced' to 300 μm layer height, later, the part was printed at 1000 °C using soda-lime glass.

39 S. Cosimo, Micron 3DP announces breakthrough in 3D printing glass materials, http://www.3ders.org/articles/20150622-micron-3dp-announces-breakthrough-in-3d-printing-glass-materials.html, 22.06.2015, accessed August 2018.

40 E. Gal-Or, MICRON3DP high resolution glass 3D printing, https://www.youtube.com/watch?v=ju6BtrIzz08, 08.12.2016, accessed August 2018.

41 J. Klein, M. Stern, G. Franchin, M. Kayser, C. Inamura, S. Dave, J. C. Weaver, P. Houk, P. Colombo, M. Yang and N. Oxman, *3D Print. Addit. Manuf.*, 2015, **2**, 92–105.

42 P.-T. Brun, C. Inamura, D. Lizardo, G. Franchin, M. Stern, P. Houk and N. Oxman, *Philos. Trans. R. Soc., A*, 2017, **375**, 20160156.

43 C. Inamura, M. Stern, D. Lizardo, P. Houk and N. Oxman, *3D Print. Addit. Manuf.*, 2018, **5**, 269–283.

44 A. Bracha, and E. Gal-Or, WIPO, PCT/IB2018/051181, WO 2018/163008 A1, 2018.

45 A. Bracha, and E. Gal-Or, WIPO, PCT/IB2018/051178, WO 2018/163006 A1, 2018.

46 A. Bracha, and E. Gal-Or, WIPO; PCT/IB2018/051179, WO 2018/163007 A1, 2018.

47 A. Greco, R. De Marco, S. Tani, D. Giacomini, P. Galletti, A. Tolomelli, E. Juaristi and L. Gentilucci, *Eur. J. Org. Chem.*, 2014, 7614–7620.

48 W. B. White and D. G. Minser, *J. Non-Cryst. Solids*, 1984, **67**, 45–59.

49 M. Hass, *J. Phys. Chem. Solids*, 1970, **31**, 415–422.

50 A. F. Chrimes, K. Khoshmanesh, P. R. Stoddart, A. Mitchell and K. Kalantar-zadeh, *Chem. Soc. Rev.*, 2013, **42**, 5880–5906.

51 M. J. Pelletier, *Appl. Spectrosc.*, 1999, **53**, 1087–1096.

52 T. Lipiäinen, J. Pessi, P. Movahedi, J. Koivistoinen, L. Kurki, M. Tenhunen, J. Yliruusi, A. M. Juppo, J. Heikkonen, T. Pahikkala and C. J. Strachan, *Anal. Chem.*, 2018, **90**, 4832–4839.

53 T. Rojalin, L. Kurki, T. Laaksonen, T. Viitala, J. Kostamovaara, K. C. Gordon, L. Galvis, S. Wachsmann-Hogiu, C. J. Strachan and M. Yliperttula, *Anal. Bioanal. Chem.*, 2016, **408**, 761–774.

54 J. Kostamovaara, J. Tenhunen, M. Kögler, I. Nissinen, J. Nissinen and P. Keränen, *Opt. Express*, 2013, **21**, 31632–31645.

55 P. D. I. Fletcher, S. J. Haswell and X. Zhang, *Electrophoresis*, 2003, **24**, 3239–3245.

